Progress In Electromagnetics Research M, Vol. 103, 221–233, 2021

Design and Analysis of Variable Leakage Flux Flux-Intensifying Motor for Improve Flux-Weakening Ability

Xiping Liu, Gaosheng Guo*, Siting Zhu, and Jianwei Liang

Abstract—This paper presents a novel variable leakage flux flux-intensifying motor (VLF-FIM) to improve flux-weakening ability. The innovation lies in the variable leakage flux property and the characteristic of $L_d > L_q$. The two characteristics can be achieved by the adoption of magnetic barriers and magnetic bridges. Consequently, the flux-weakening ability is enhanced. Then, the topology structure and operation principle of the proposed machine are introduced. Based on the two-dimensional finite element method (2DFEM), the performances of the proposed motor are analyzed and compared with the conventional interior permanent magnet motor (CIPMM) in detail. The performances mainly include torque, flux-weakening ability, constant power speed range (CPSR), irreversible demagnetization risk of the PM, structural strength, etc. Finally, the results show that the proposed motor has some advantages, such as good flux-weakening ability, a wide constant power range, and a large high-efficiency area. In addition, it verifies the effectiveness of the proposed method in improving the flux-weakening ability of the motor.

1. INTRODUCTION

Permanent magnet synchronous machines (PMSMs) have obvious advantages in high torque density, high power density, and high efficiency [1]. Hence, PMSM has become a research hotspot and widely researched and applied in electric vehicles (EVs) and hybrid electric vehicles (HEVs) [2]. However, the air-gap magnetic field of PMSM is difficult to adjust due to the inherent properties of PM [3]. Thus, it is difficult for the motor to achieve high-speed constant power operation [4]. To extend the operating speed range, the machine usually injects a large d-axis current id to weaken the air-gap magnetic field [5]. However, the method inevitably brings some problems, such as copper loss, and the risk of irreversible demagnetization of PMs will increase [6].

In the past few years, some variable flux motors are proposed to improve the flux-weakening ability. Hybrid-excited (HE) machines are proposed and researched in [7–9]. In HE machines, the magnetic field generated by the PMs and field coils (FCs) can be enhanced and weakened by controlling the amplitude of the current of the excitation coil. Thus, the HE machines inherit the advantages of the high torque/power density of PM machines and flexible flux regulation ability of the wound-field machines [9]. In [10], a variable flux memory machine (VFMM) has been proposed to achieve wide CPSR. The VFMM is adopted with a low coercive force permanent magnet (LCF-PM), and the magnetization state of the LCF-PM can be regulated by injecting a current pulse to remagnetize or demagnetize [11]. The current pulses are energized by the DC magnetizing coils, which facilitates the online magnetization control [12]. Consequently, high torque and wide speed range can be achieved by controlling the current pulse [13]. In [14], mechanical-variable-flux PM machines (MVF-PMMs) are presented and studied, where the mechanical flux-adjusting device is attached to the rotor. Compared with electrical variable flux techniques, MVF-PMM has the advantage that the magnetic field can be adjusted flexibly by the

Received 2 July 2021, Accepted 3 August 2021, Scheduled 9 August 2021
* Corresponding author: Gaosheng Guo (1400681644ggs@gmail.com).
The authors are with the School of Electrical and Automation, Jiangxi University of Science and Technology, Ganzhou, China.

equipped mechanical flux-adjusting device [15]. This device is driven by centrifugal force to achieve magnetic field weakening [16], and its main method of flux weakening is to increase the leakage flux by adopting a unique structure. Thus, this type of motor can easily achieve large torque at low speed and has a strong flux-weakening ability at high speed. In [17], a flux-intensifying interior permanent magnet (FI-IPM) motor is proposed. By setting a reasonable magnetic barrier on the d-axis and q-axis flux paths of the rotor, the motor possesses the unique characteristic of d-axis inductance L_d larger than the q-axis inductance L_q. This property enables the FI-IPM motor to obtain positive reluctance at a positive flux-intensifying current i_d [18]. Compared with the maximum torque of the conventional IPM motor achieved at negative flux-weakening current i_d, the risk of irreversible demagnetization of the FI-IPM motor is lower [19]. Besides, the flux-intensifying effect can reduce the flux-weakening current at a high speed [20]. In [21], a variable leakage flux interior permanent magnet (VLM-IPM) motor is proposed. The motor has a leakage flux path between magnet poles, and the leakage flux of the path can be controlled by the q-axis current [22]. At the rated speed, the q-axis current is increased to reduce the leakage flux and thus improve the output torque; at the high speed, the leakage flux path is used to reduce the air gap magnetic density, so as to improve flux-weakening ability and reduce flux-weakening current [23].

In this paper, a novel VLF-FIM is proposed. The VLF-FIM combines the advantages of the FI-IPM motor and VLF-IPM motor, which owns a unique characteristic of $L_d > L_q$ and variable leakage flux property. The topology structure and operation principle of the proposed motor are introduced. The electromagnetic performances and structural strength are analyzed and compared. The results can verify that the flux-weakening ability of the proposed motor can be improved by the design method.

2. TOPOLOGY AND PRINCIPLES OF MACHINE

2.1. Machine Topology

In this paper, a conventional interior permanent magnet motor (CIPMM) with a V-shaped PM is selected as a comparison motor, and the VLF-FIM is proposed based on the CIPMM. The topologies of the CIPMM and VLF-FIM are shown in Figure 1. The two motors have a 48-slot/8-pole and different rotor structures. Besides, the rotor topology evolution from the CIPMM to VLF-FIM is shown in Figure 2, which includes the evolution of magnetic barriers and PMs. As seen from the figure, to realize the variable leakage flux property, a leakage flux path is established on the q-axis of the VLF-FIM. To obtain the characteristic of $L_d > L_q$, the magnetic barriers and magnetic bridges are reasonably designed, in which the magnetic barrier is to reduce L_q, and the magnetic bridge is to increase L_d. Consequently, the variable leakage flux property and the characteristic of $L_d > L_q$ of the proposed motor can be realized by innovative design. It means that the VLF-FIM has the advantage of inheriting VLFM and FIM. According to the design theory of the IPMM, the key design parameters of the two motors are given in Table 1.

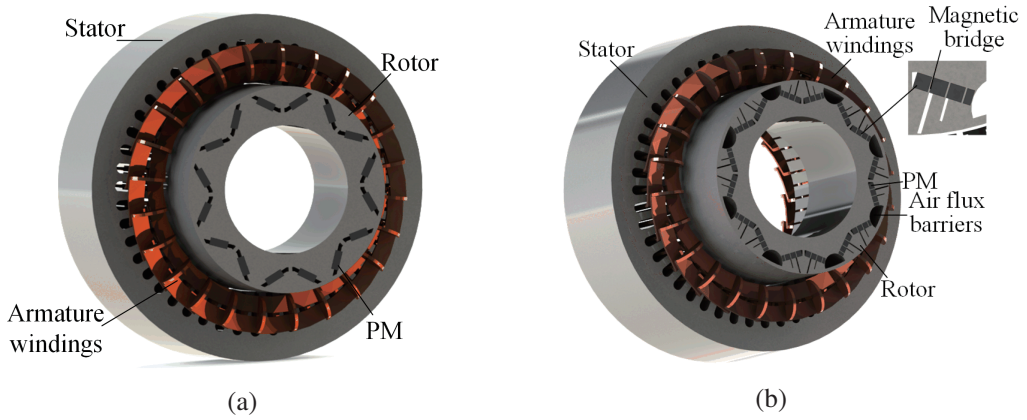

Figure 1. Topologies of the two motors. (a) CIPMM. (b) VLF-FIM.

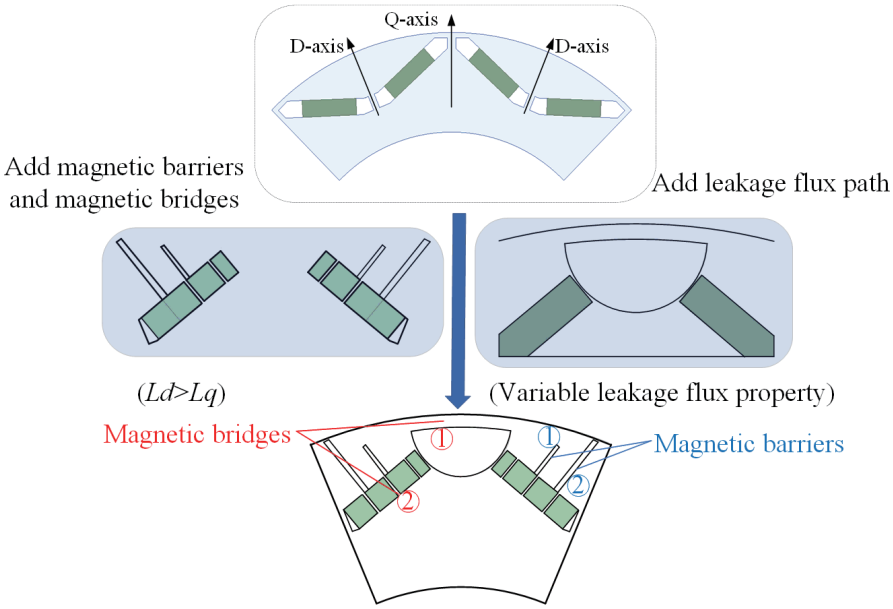

Figure 2. Rotor evolution from the conventional interior PM motor to the VLF-FIM.

Table 1. Key design parameters of the two motors.

Items	CIPMM	VLF-FIM
Rated output power (kW)	10	10
Rated speed (rpm)	1200	1200
Stator inner diameter D_{si} (mm)	161.9	161.9
Air-gap length (mm)	0.75	0.75
Active stack length L_{axis} (mm)	83.82	83.82
Numbers of turns	18	18
PM material	N36Z_20 (1.03 T, 920 kA/m)	N36Z_20 (1.03 T, 920 kA/m)
PM width/ thickness (mm)	17.5/5	17.5/5
Widen of magnetic bridge 1,2 (mm)	/	2.5/0.5
Widen of magnetic barrier 1,2 (mm)	/	0.6/1

2.2. Operation Principles

Compared with the CIPMM, the VLF-FIM has the unique characteristic of $L_d > L_q$ and variable leakage flux property to improve the flux-weakening ability. To analyze the difference between the two motors and the two characteristics of the proposed motor, the simplified d-axis and q-axis equivalent magnetic circuits of the CIPMM and VLF-FIM are shown in Figures 3(a) and 3(b), respectively. Compared with the equivalent magnetic circuits of the CIPMM, the d-axis magnetic circuit of the VLF-FIM has one more leakage magnetic circuit due to leakage flux bypass, and the reluctance of the q-axis magnetic circuit of the VLF-FIM increases due to the air-gap magnetic barrier. Based on this simplified equivalent magnetic circuit, two characteristics of the proposed motor will be analyzed below:

Firstly, the characteristic of $L_d > L_q$ is analyzed. The magnetic saturation effect of PMs in this analysis model is neglected. Hence, the static d-axis inductance and q-axis inductance can be expressed

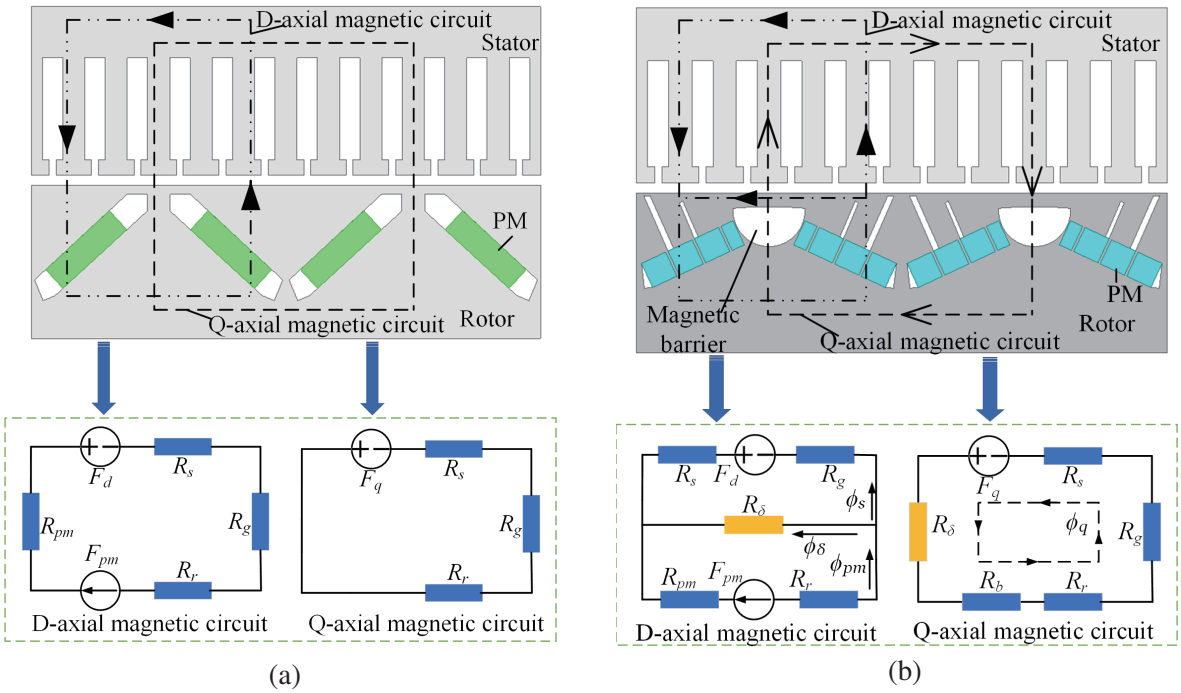

Figure 3. Simplified d-axis and q-axis equivalent magnetic circuits of the two motors. (a) CIPMM. (b) VLF-FIM.

as below:

$$\begin{cases} Ld = \dfrac{N^2}{Rs + Rg + R1} \\ Lq = \dfrac{N^2}{Rs + Rg + Rr + Rb + R\delta} \\ Fd = Nid, Fq = Niq \\ R1 = \dfrac{R\delta(Rpm + Rr)}{(Rpm + Rr + R\delta)} \end{cases} \tag{1}$$

where N is the number of turns of winding; R_s, R_g, R_r, R_{pm}, R_δ, R_b are the reluctances of the stator, air-gap, rotor, PM, leakage flux bypass, magnetic barrier; F_d and F_q are the stator magnetomotive forces of d-axis and q-axis. According to Equation (1), to realize the characteristic of $L_d > L_q$, the proposed motor reduces L_q by adding a magnetic barrier on the q-axis magnetic circuit and increases L_d by setting a magnetic bridge on the PM.

Based on the magnetic circuit of VLF-FIM, the variable leakage flux property is derived as follows:

$$\begin{cases} \phi\delta = \phi pm - \phi s = \dfrac{(Rg + Rs)\, Fpm - RsFd}{R\delta\,(Rr + Rpm) + (R\delta + Rr + Rpm)\,(Rs + Rg)} \\ R\delta = \dfrac{l}{u\delta A} = \dfrac{\mathrm{N}iq}{\phi q} - Rs - Rg - Rb - Rr \end{cases} \tag{2}$$

where F_{pm} is the magnetomotive force of PM; ϕ_s, ϕ_{pm}, ϕ_δ, ϕ_q are the magnetic fluxes of the stator, PM, leakage flux bypass, q-axis, respectively; u_δ is the permeability of the leakage flux bypass; l and A are the lengths and cross-sectional area of the leakage flux bypass. According to Equation (2), it can be found that ϕ_δ is mainly affected by R_δ. Moreover, the simple schematic of the variable flux principle is shown in Figure 4. As seen from the figure, the variable leakage flux property is realized by controlling the permeability of the leakage flux bypass. As the q-axis current increases, the permeability of the leakage flux bypass decreases. As a result, the leakage flux of the leakage flux bypass flows to the stator. When the current reaches a certain value, the magnetic saturation degree of the magnetic leakage flux

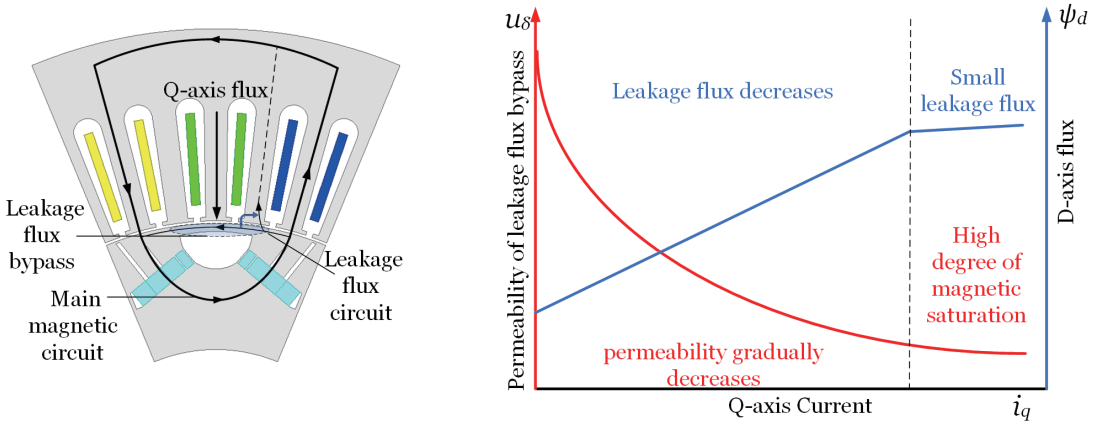

Figure 4. Simple schematic of the variable flux principle.

bypass is very high. Thus, the permeability changes little, and most of the leakage flux flows to the stator, which can achieve large permanent magnet torque output. The corresponding d-axis magnetic flux ψ_d can be expressed as follows:

$$\begin{cases} \psi d = Ldid + \psi(iq) + \psi pm\_0 \\ \psi m = \psi(iq) + \psi pm\_0 \end{cases} \tag{3}$$

where ψ_{pm_0} is a no-load PM flux linkage, and $\psi_{(iq)}$ is a flux linkage affected by the q-axis current i_q. Besides, the maximum speed $\psi_{\max}$ of the motor and flux-weakening ability λ can be expressed as

$$\begin{cases} \omega \max = \dfrac{Ulim}{p(\psi pm\_0 - LdIlim)} \\ \lambda = \dfrac{\psi pm\_0}{Ld} \end{cases} \tag{4}$$

where U_{lim} and I_{lim} are the limit values of voltage and armature current; p is the number of pole pairs. The proposed motor owns the variable leakage flux property and the characteristic of $L_d > L_q$, which can decrease ψ_{pm_0} and increase L_d. It means that the two characteristics can improve the flux weakening ability and broaden the speed range

3. PERFORMANCES ANALYSIS AND COMPARISON

3.1. No-Load Performance

Under no load, the air-gap flux density and back-EMF are analyzed and shown in Figure 5. Figure 5(a) shows the radial air-gap flux density curves of the two motors. It can be found that the peak value of the air-gap flux density of the VLF-FIM is lower than that of the CIPMM. Besides, in Figure 5(b), the no load back-EMF waveforms of the two motors are shown at the speed of 1000 rpm. It can be observed that the magnitude of the back-EMF of the proposed motor is smaller than that of the CIPMM. It is mainly due to the leakage flux bypass of the VLF-FIM, which can effectively weaken the air gap magnetic density. Based on the fast Fourier transform method, the corresponding harmonic analysis is shown in Figure 6(c). As seen from the figure, the three-order, five-order, and nine-order harmonics of the CIPMM are larger than that of the VLF-FIM. The total harmonic distortion (THD) of the CIPMM and VLF-FIM is 17.6% and 7.2%. It means that the back-EMF of the VLF-FIM is more sinusoidal.

3.2. Flux Characteristic

The flux characteristic is an important aspect of the motor, which has a significant influence on the PM torque and capability of flux weakening. Thus, it is necessary to analyze the flux distribution at different operating conditions.

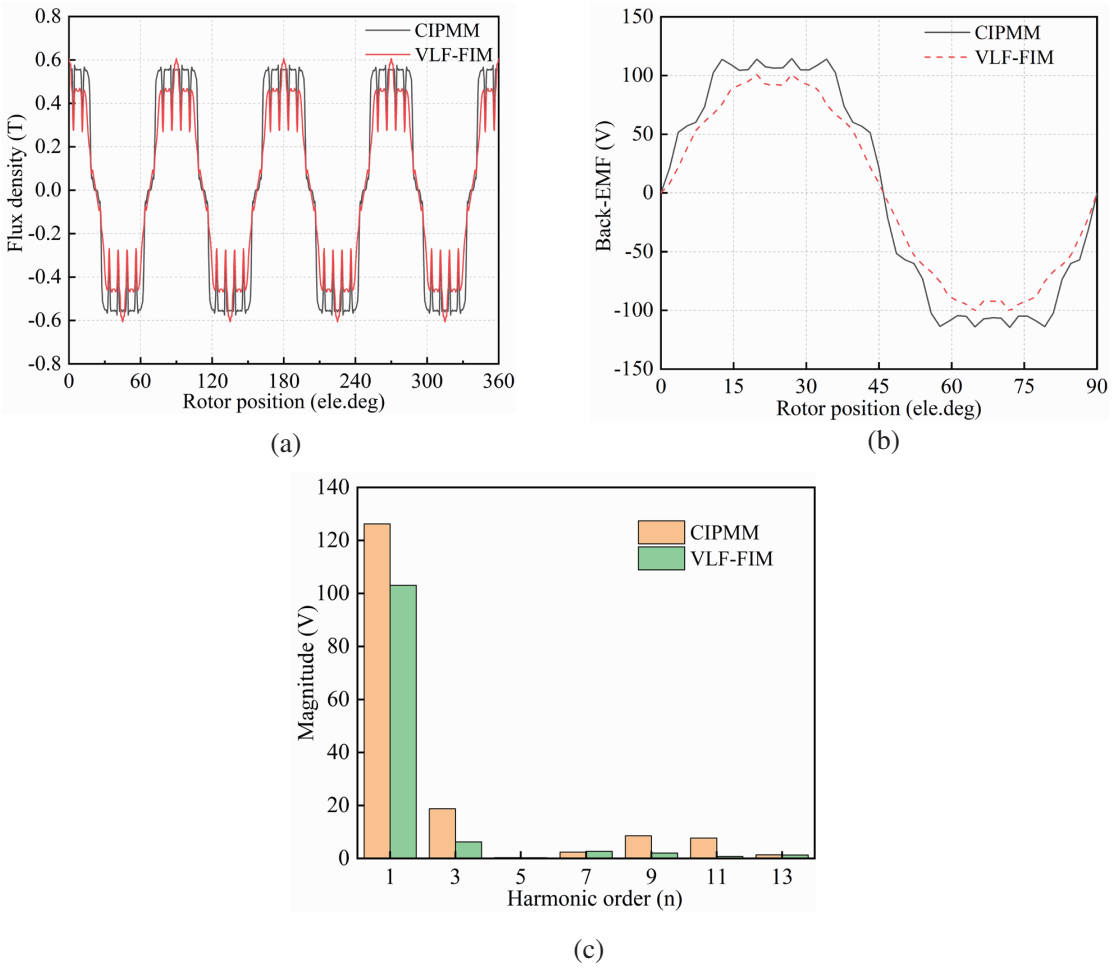

Figure 5. No-load characteristics. (a) Air-gap flux density. (b) Back-EMF waveforms. (c) Harmonic component of the back-EMFs.

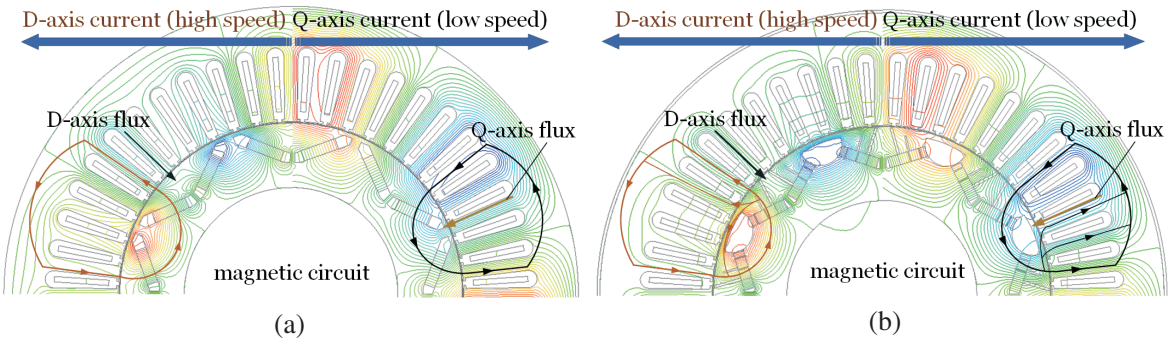

Figure 6. Flux distributions under the *d*-axis current and *q*-axis current. (a) CIPMM. (b) VLF-FIM.

Figure 6 shows the flux distributionS of the two motors under the *d*-axis current and *q*-axis current. In Figure 6(a), it can be seen that a large number of magnetic fluxES pass through the stator under the *q*-axis current, which can obtain large PM torque. When the *d*-axis current is applied, the magnetic field is significantly weakened, thus increasing the speed range. On the other hand, in Figure 6(b), when the *q*-axis current is injected, the magnetic flux is toward the stator teeth path instead of the bypass between magnet poles because the leakage flux path reaches magnetic saturation, which means

that the PM torque can improve. Under d-axis current, the part of the PM flux forms a loop through the leakage flux path because there is no influence of the q-axis current. Therefore, compared with the CIPMM, the VLF-FIM can obtain a better flux-weakening capacity.

Moreover, to further investigate the variable leakage flux property of the VLF-FIM, the relative permeability u of the leakage flux bypass is analyzed, and the two observation points are selected in the bypass as shown in Figure 7. Figure 8 shows the detailed variations of the relative permeabilities of the two observation points and d-axis flux under different currents. As seen from the figure, as the current increases, the relative permeabilities of the two observation points decrease gradually, and the d-axis flux increases. It verifies the validation of controlling flux leakage by q-axis current.

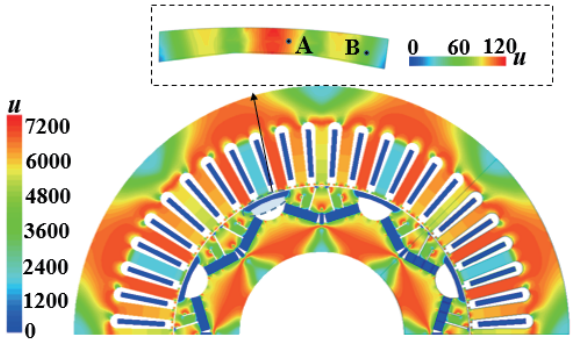

Figure 7. Relative permeability distribution and the selection of two observation points.

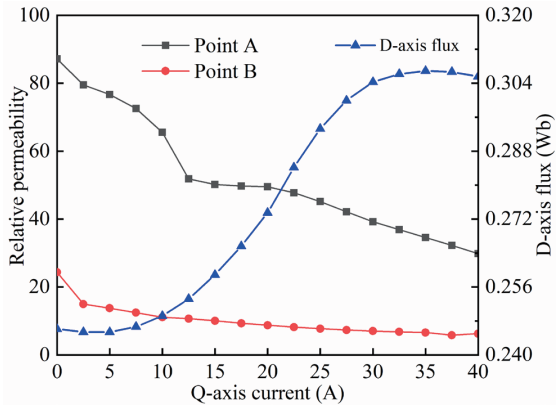

Figure 8. Variations of relative permeabilities of the two observation points and d-axis flux under different currents.

3.3. Inductance Characteristics

Under different currents, the inductance characteristics of the two motors are investigated and shown in Figure 9. In Figure 9(a), L_d is smaller than that of L_q, and L_d and L_q of the CIPMM decrease with the current increase, but L_d changes little. Thus, the difference value between L_q and L_d is getting smaller. In Figure 9(b), the characteristics of $L_d > L_q$ are maintained with the current increase, which

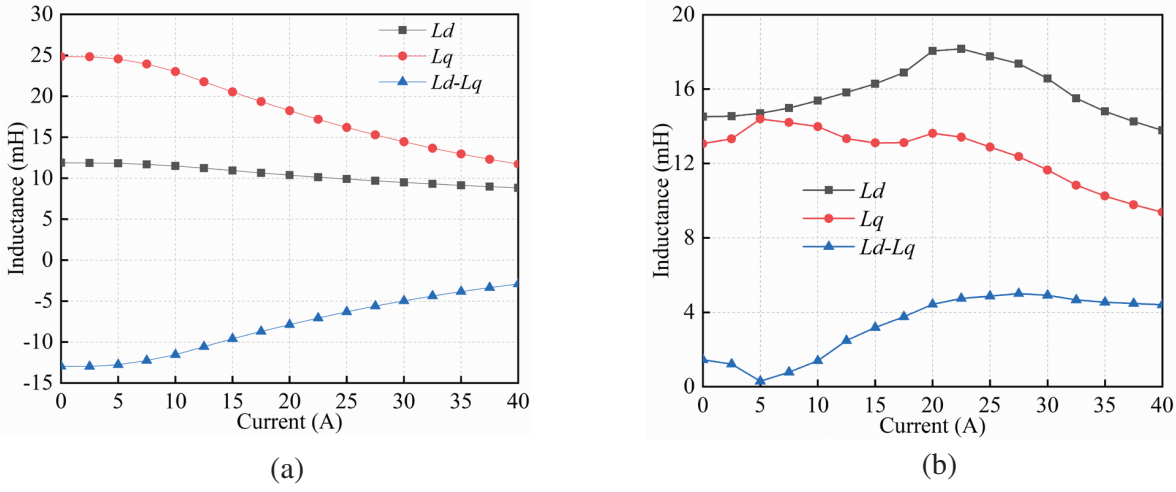

Figure 9. Inductance variation characteristics of the two motors under different currents. (a) CIPMM, (b) VLF-FIM.

results from the q-axis magnet barrier and d-axis magnet bridge. Consequently, the positive reluctance torque of the VLF-FIM can be obtained at a positive d-axis current. Besides, it can be found that L_d of the VLF-FIM is larger than that of the CIPMM, and L_q of the VLF-FIM is smaller than that of the CIPMM. It has proved that it is feasible to increase the d-axis inductance and reduce the q-axis inductance by adding magnetic barriers and magnetic bridges.

3.4. Torque Characteristics

The electromagnetic torque of the IPMSM can be expressed as:

$$T = \frac{3P}{2}\left[\psi miq + (Ld - Lq)idiq\right] \tag{5}$$

According to Equation (5), the electromagnetic torque can be divided into PM torque and reluctance torque. The relationship between torque and the current of i_q is shown in Figure 10(a), where the d-axis current i_d is set as 0 A, so the only PM torque output. It can be found that the torque of the CIPMM is an almost linear variation with the current increase. However, the VLF-FIM is a nonlinear variation, which demonstrates a quadratic equation. It is mainly caused by leakage flux property. Besides, Figure 10(b) shows the relationship between the current angles and torques of the two proposed motors. The maximum torque of the VLF-FIM is realized in a positive d-axis current i_d, while the CIPMM is achieved in a negative d-axis current i_d.

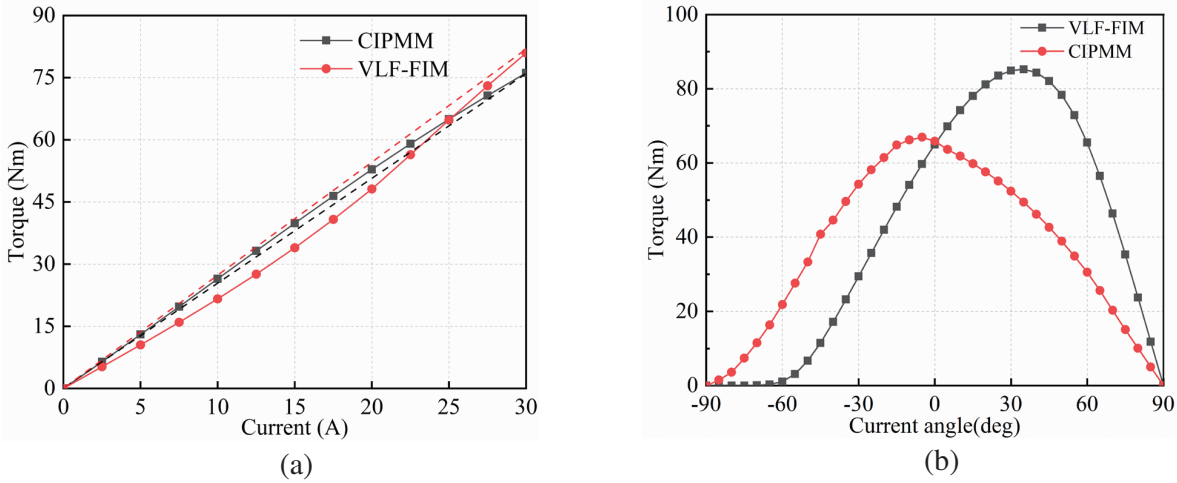

Figure 10. Torque characteristics of the two motors. (a) Variation characteristics of torque versus q-axis current. (b) Output torque versus current angle.

3.5. Evaluating the Irreversible Demagnetization Risk

It is well known that the irreversible demagnetization of PM will affect the performance of the motor, which main includes output torque. Thus, the magnetization state of PM is evaluated by finite-element analyses (FEA).

To analyze the magnetization state of the permanent magnet effectively, some observation points are selected in each motor, and the corresponding magnetization state is analyzed. Figure 11 shows the magnet density distributions of the two motors under no load. In Figure 12(a), it can be found that the three observation points of the CIPMM have almost the same flux density of 1.12 T. The magnetization state of the observation points of the VLF-FIM is shown in Figure 12(b), and it is observed that the magnetic density of the four points is also around 1.12 T. It means that the PM of the two motors has the same magnetization state.

Under the rated output torque, the magnetization state of the observation points is analyzed and shown in Figure 13. In Figure 13(a), it can be seen that the flux densities of point B and point C have

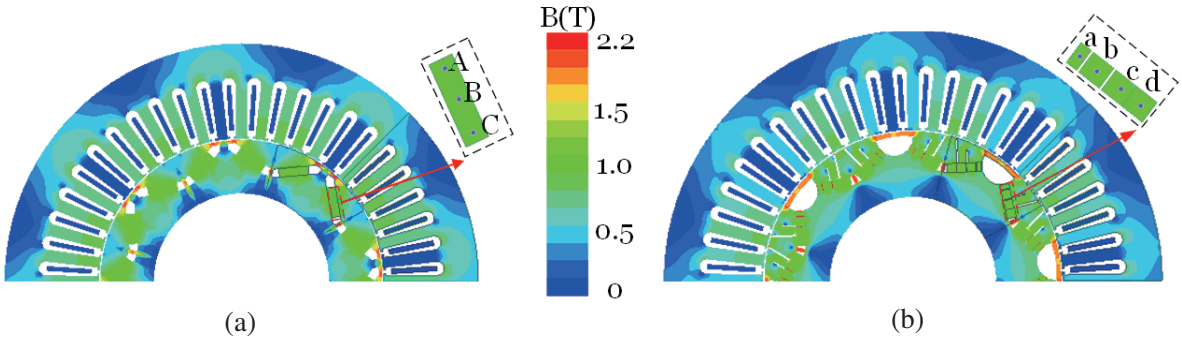

Figure 11. Flux density distributions under no load. (a) CIPMM. (b) VLF-FIM.

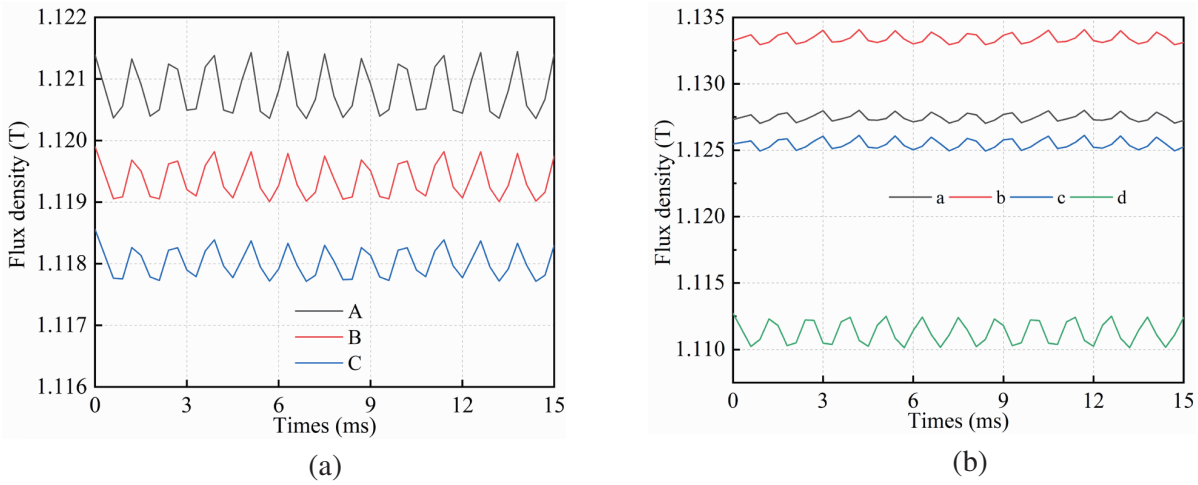

Figure 12. Flux density variations of the observation points of the two motors under no load. (a) CIPMM. (b) VLF-FIM.

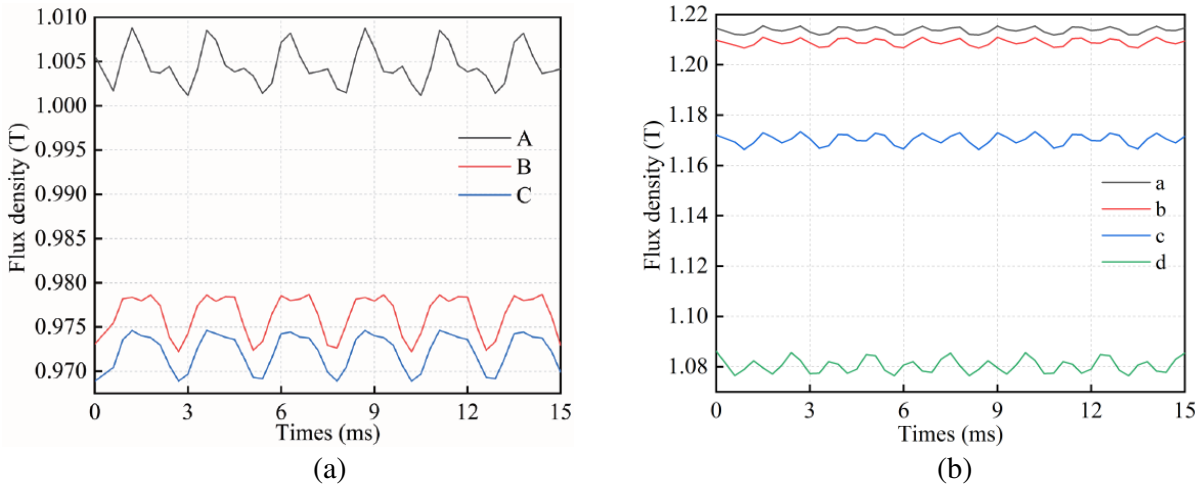

Figure 13. Flux density variations of the observation points of the two motors under load. (a) CIPMM. (b) VLF-FIM.

the same value of 0.98 T, which is slightly less than that of point A of 1 T. As shown in Figure 13(b), the magnetic densities of point a, point b, and point c are approximately 1.2 T, which is larger than that of point d of 1.08 T. Compared with no load, the flux density of the observation points of the CIPMM is decreased, while the VLF-FIM is increased. The reason for this result is that the rated torque of VLF-FIM operates in the flux-intensity region due to the characteristic of $L_d > L_q$, while CIPMM operates in the flux-weakening region due to the characteristic of $L_d < L_q$. It means that a lower risk of irreversible demagnetization in the proposed motor can be obtained.

3.6. Torque and Output Power Versus Speed Characteristics

The proposed motor is designed to achieve a wider range of speeds, so it is necessary to study the characteristics of torque and output power with the variation of speed.

The torque-speed envelops and output power-speed envelops of the two motors are shown in Figure 14, where the maximum torque per ampere (MTPA) control strategy is adopted. It can be seen from Figures 14(a) and 14(b) that the VLF-FIM owns a wider speed range and wider constant power range than the CIPMM, and the output powers of the two motors reach nearly 10 kW. However, it can be observed that the output torque is larger than that of the VLF-FIM. It means that the proposed method can effectively improve the capacity of flux-weakening to widen the speed range but will decrease the output torque of the motor.

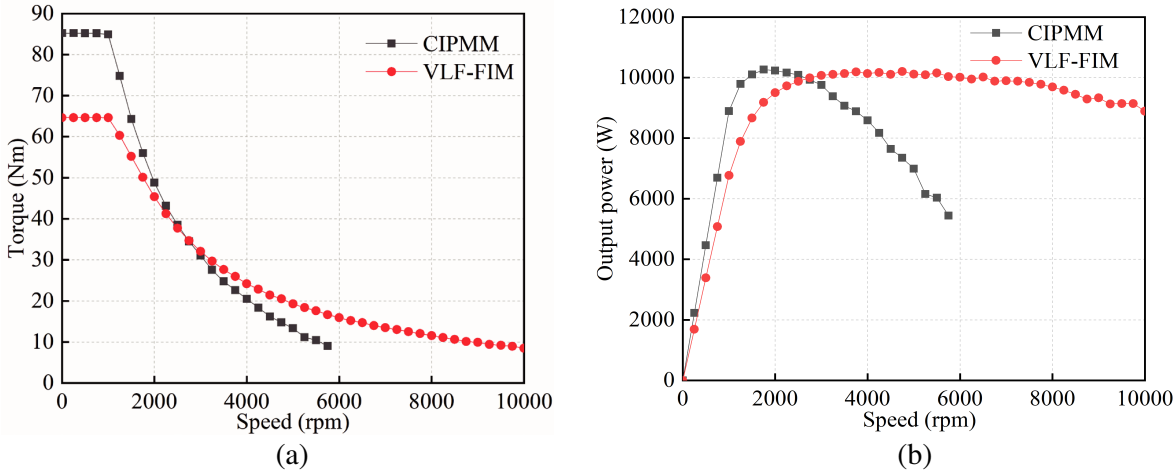

Figure 14. Torque-speed and output power-speed characteristics. (a) Torque-speed envelops. (b) Output power-speed envelops.

According to the above analysis, the speed range of the proposed motors is much larger than that of CIPMM. It means that the speed range of the motor can be extended by the variable leakage flux property and the characteristic of $L_d > L_q$.

3.7. Iron Loss and Efficiency Analysis

In this section, the iron loss and efficiency of the two motors are analyzed by FEA. The loss of the motor main including iron loss, copper loss, and mechanical loss. The iron loss of the two motors is selected to evaluate due to variable leakage flux characteristics that can affect iron loss. The iron loss consists of hysteresis loss (P_h) and eddy current loss (P_e), and can be calculated by Equation (6),

$$Piron = Ph + Pe = khfB_m^{\alpha} + kefB_m^2 \tag{6}$$

where f is the fundamental frequency; k_h and α are the hysteresis coefficient; k_e is the eddy current coefficient; B_m is the magnetic density value. According to the equation, it can be found that the iron loss is determined by the frequency and magnetic flux density in the iron core. Figure 15 shows the iron

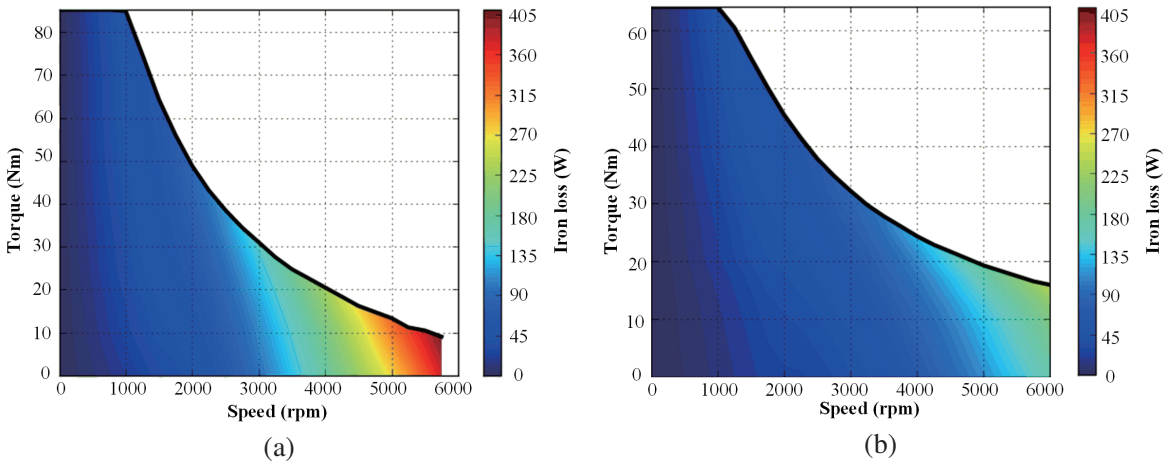

Figure 15. Iron losses of the two motors. (a) CIPMM. (b) VLF-FIM.

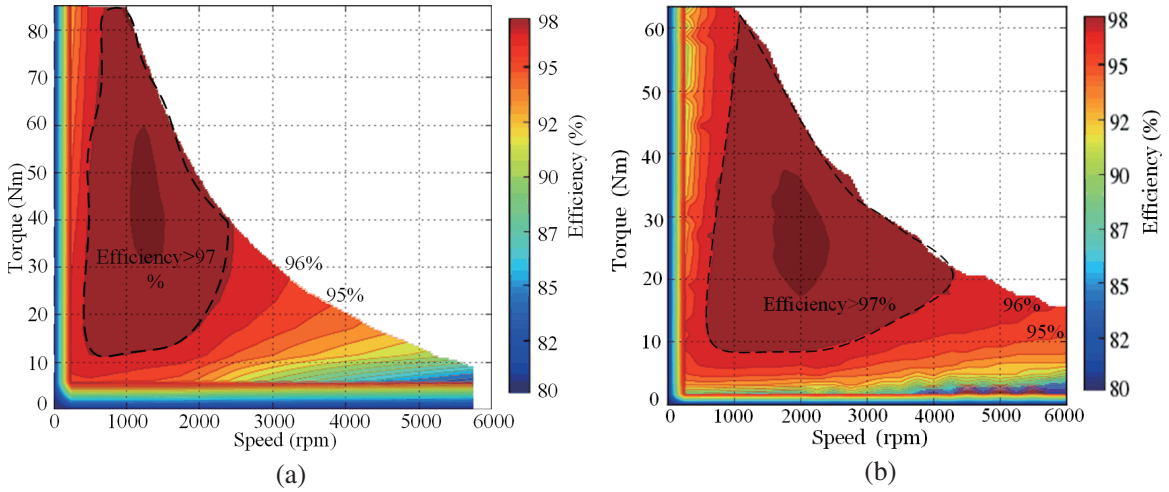

Figure 16. Efficiency maps of the two motors. (a) CIPMM. (b) VLF-FIM.

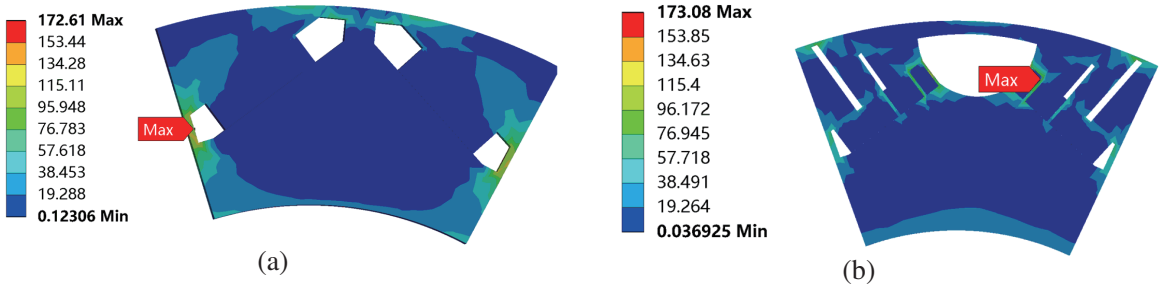

Figure 17. Stress analysis of the two motors at speed of 10000 rpm. (a) CIPMM. (b) VLF-FIM.

loss of the two motors. As seen from the two figures, at low speeds, the iron losses of the two motors are similar; however, at high speed, it is obvious that the iron loss of CIPMM is higher than that of VLF-FIM. This is because the variable leakage flux property can effectively weaken the magnetic flux density.

Figure 16 shows the efficiency maps of CIPMM and VLF-FIM, where the same rated current is

applied. Comparing the two figures, it is found that the 97% efficiency area of the proposed motor is wider than that of CIPMM, because the variable leakage flux characteristic of the proposed motors can reduce the iron loss and flux-weakening current.

3.8. Stress Analysis

The mechanical strength of the rotor is required to be able to operate safely at high speeds. Thus, the stress analysis of the two motors is essential. Figure 17 shows the results of the stress analysis of the two motors at the speed of 10000 rpm. It can be found that the maximum stress values of the two motors reach nearly 173 Mpa, which is far less than the yield strength of silicon steel 450 Mpa. It means that the rotor structure of the VLF-FIM can withstand centrifugal force at high speeds.

4. CONCLUSION

In this paper, a novel VLF-FIM has been proposed. This proposed machine possesses the variable leakage flux property and characteristic of $L_d > L_q$ by adopting magnetic barriers and magnetic bridges. Based on 2DFEA, the electromagnetic performances of the CIPMM and VLF-FIM are compared and analyzed. Benefiting from the characteristic of $L_d > L_q$, the VLF-FIM can operate with flux-intensifying current at rated speed, which can effectively reduce the risk of permanent magnet demagnetization. Moreover, owing to the relatively larger L_d and variable leakage flux property, the flux-weakening ability can be improved. Thus, the CPSR and high-efficiency area of the VLF-FIM is wider than that of the CIPMM. And the designed motor meets the strength requirements. Based on the above performance analysis and comparison, the proposed motor is more suitable for EV application.

ACKNOWLEDGMENT

This work was supported in part by the National Natural Science Foundation of China under grant No. 52067008 and No. 51767009, in part by the Plan Project of Jiangxi Province of P. R. China under grant No. 20181BAB206035, and in part by the Program of Qingjiang Excellent Young Talents, Jiangxi University of Science and Technology (JXUST).

REFERENCES

1. Shi, Z., X. D. Sun, Y. F. Cai, and Z. B. Yang, "Torque analysis and dynamic performance improvement of a PMSM for EVs by skew angle optimization," *IEEE Transactions on Applied Superconductivity*, Vol. 29, No. 2, 1–5, 2019.
2. Jayarajan, R., N. Fernando, and I. U. Nutkani, "A review on variable flux machine technology: Topologies, control strategies and magnetic materials," *IEEE Access*, Vol. 7, No. 4, 70141–70156, 2019.
3. Thike, R. and P. Pillay, "Characterization of a variable flux machine for transportation using a vector-controlled drive," *IEEE Transactions on Transportation Electrification*, Vol. 4, No. 2, 494–505, 2018.
4. Kim, J., D. Kim, G. Park, Y. Kim, and S. Jung, "Analysis and design of SPM type variable flux memory motor considering demagnetization characteristic of permanent magnet," *IEEE Transactions on Applied Superconductivity*, Vol. 28, No. 3, 1–5, 2018.
5. Zhu, X., S. Yang, Y. Du, Z. Xiang, and L. Xu, "Electromagnetic performance analysis and verification of a new flux-intensifying permanent magnet brushless motor with two-layer segmented permanent magnets," *IEEE Transactions on Magnetics*, Vol. 52, No. 7, 1–4, 2016.
6. Sun, A., J. Li, R. Qu, J. Chen, and H. Lu, "Rotor design considerations for a variable-flux flux-intensifying interior permanent magnet machine with improved torque quality and reduced magnetization current," *2015 IEEE Energy Conversion Congress and Exposition (ECCE)*, 784–790, 2015.

7. Yu, J., C. Liu, Z. Song, and H. Zhao, "Permeance and inductance modeling of a double-stator hybrid-excited flux-switching permanent-magnet machine," *IEEE Transactions on Transportation Electrification*, Vol. 6, No. 3, 1134–1145, 2020.
8. Yu, J. and C. Liu, "Multi-Objective optimization of a double-stator hybrid-excited flux-switching permanent-magnet machine," *IEEE Transactions on Energy Conversion*, Vol. 35, No. 1, 312–323, 2020.
9. Cao, L., K. T. Chau, C. H. T. Lee, and W. Lam, "Design and analysis of a new parallel-hybrid-excited machine with harmonic-shift structure," *IEEE Transactions on Industrial Electronics*, Vol. 67, No. 3, 1759–1770, 2020.
10. Yang, H., H. Lin, Y. Li, H. Wang, S. Fang, and Y. Huang, "Analytical modeling of switched flux memory machine," *IEEE Transactions on Magnetics*, Vol. 54, No. 3, 1–5, 2018.
11. Xie, Y., Z. Ning, and Z. Ma, "Comparative study on variable flux memory machines with different arrangements of permanent magnets," *IEEE Access*, Vol. 8, No. 2, 164304–164312, 2020.
12. Wei, L. and T. Nakamura, "Design and optimization of a partitional stator flux-modulated memory machine," *IEEE Transactions on Magnetics*, Vol. 56, No. 4, 1–5, 2020.
13. Yang, H., H. Lin, and Z. Q. Zhu, "Recent advances in variable flux memory machines for traction applications: A review," *CES Transactions on Electrical Machines and Systems*, Vol. 2, No. 1, 34–50, 2018.
14. Liu, X. P., Y. L. Zou, and T. Z. Sun, " Design and performance analysis of a novel mechanical fluxadjusting interior permanent magnet motor," *Electrical Engineering*, Vol. 103, No. 3, 1515–1524, 2021.
15. Tessarolo, A., M. Mezzarobba, and R. Menis, "Modeling, analysis, and testing of a novel spoke-type interior permanent magnet motor with improved flux weakening capability," *IEEE Transactions on Magnetics*, Vol. 51, No. 4, 1–10, 2015.
16. Zhu, Z. Q., M. M. J. Al-Ani, X. Liu, and B. Lee, "A mechanical flux weakening method for switched flux permanent magnet machines," *IEEE Transactions on Energy Conversion*, Vol. 30, No. 2, 806–815, 2015.
17. Limsuwan, N., T. Kato, K. Akatsu, and R. D. Lorenz, "Design and evaluation of a variable-flux flux-intensifying interior permanent-magnet machine," *IEEE Transactions on Industry Applications*, Vol. 50, No. 2, 1015–1024, 2014.
18. Limsuwan, N., Y. Shibukawa, D. D. Reigosa, and R. D. Lorenz, "Novel design of flux-intensifying interior permanent magnet synchronous machine suitable for self-sensing control at very low speed and power conversion," *IEEE Transactions on Industry Applications*, Vol. 47, No. 5, 2004–2012, 2011.
19. Zhao, X., B. Kou, L. Zhang, and H. Zhang, "Design and analysis of permanent magnets in a negative-salient permanent magnet synchronous motor," *IEEE Access*, Vol. 8, No. 4, 182249–182259, 2020.
20. Zhang, L., X. Zhu, J. Gao, and Y. Mao, "Design and analysis of new five-phase flux-intensifying fault-tolerant interior-permanent-magnet motor for sensorless operation," *IEEE Transactions on Industrial Electronics*, Vol. 67, No. 7, 6055–6065, 2020.
21. Kato, T., M. Minowa, H. Hijikata, K. Akatsu, and R. D. Lorenz, "Design methodology for variable leakage flux ipm for automobile traction drives," *IEEE Transactions on Industry Applications*, Vol. 51, No. 5, 3811–3821, 2015
22. Fan, W., X. Zhu, L. Quan, W. Wu, L. Xu, and Y. Liu, "Flux-weakening capability enhancement design and optimization of a controllable leakage flux multilayer barrier pm motor," *IEEE Transactions on Industrial Electronics*, Vol. 68, No. 9, 7814–7825, 2021.
23. Aoyama, M. and T. Noguchi, "Study and experimental performance evaluation of flux intensifying PM motor with variable leakage magnetic flux," *Electrical Engineering in Japan*, Vol. 207, No. 4, 36–54, 2019.